Basic design considerations for a frequency step-tunable electron cyclotron wave system to suppress NTMs in DEMO

Chuanren Wu[a], Gaetano Aiello[b], Konstantinos A. Avramidis[a], Alessandro Bruschi[c], Emiliano Fable[d], Thomas Franke[d,e], Gerd Gantenbein[a], Saul Garavaglia[c], Gustavo Granucci[c], Stefan Illy[a], Filip Janky[d], John Jelonnek[a], Ondrej Kudlacek[d], Alessandro Moro[c], Emanuele Poli[d], Tobias Ruess[a], Theo Scherer[b], Raphael Schramm[d], Mattia Siccinio[d,e], Antti Snicker[f], Dirk Strauß[b], Guillermo Suárez López[d], Giovanni Tardini[d], Manfred Thumm[a], Minh Quang Tran[g], Hartmut Zohm[d]

[a] *Institute for Pulsed Power and Microwave Technology, Karlsruhe Institute of Technology, Hermann-von-Helmholtz-Platz 1, 76344 Eggenstein-Leopoldshafen, Germany*
[b] *Institut für Angewandte Materialien, Karlsruhe Institute of Technology, Hermann-von-Helmholtz-Platz 1, 76344 Eggenstein-Leopoldshafen, Germany*
[c] *Institute for Plasma Science and Technology, National Research Council of Italy, Via Roberto Cozzi, 53, 20125 Milano, Italy*
[d] *Max-Planck-Institut für Plasmaphysik, Boltzmannstrasse 2,85748 Garching, Germany*
[e] *EUROfusion Consortium, Boltzmannstrasse 2,85748 Garching, Germany*
[f] *Aalto University, PO BOX 11000, 00076 Aalto, Finland*
[g] *Swiss Plasma Center, École polytechnique fédérale de Lausanne, Station 13, CH-1015 Lausanne, Switzerland*

Abstract

An Electron Cyclotron Wave (ECW) system will be used in the European DEMO for the stabilization of Neoclassical Tearing Modes (NTMs). In order to avoid movable mirrors in the harsh environment close to the plasma and to simplify the NTM launcher integration, the tuning of the ECW deposition location can be achieved by launching frequency-tunable ECWs from fixed mirrors while the frequency is tuned in discrete steps of 2–3 GHz. An overview of the frequency step-tunable ECW system for NTM stabilization is presented. The design considerations are discussed based on the current DEMO baseline parameters and the status of technologies. A simulation of NTM stabilization with an idealized frequency tunable ECW system on an analytical NTM model is shown. The simulation takes into account a realistic tuning speed based on the present technology and considers the current NTM launcher configurations in DEMO. A simple sweeping strategy is adapted for the control of frequency. Various uncertainties, which will affect the feasibility, need to be further investigated.

Keywords:
DEMO, neoclassical tearing mode, electron cyclotron wave, heating, current drive, frequency steering, frequency step-tunable gyrotron

1. Introduction

The deposition of the Electron Cyclotron Wave (ECW) power occurs at the EC resonance, which is capable of creating local heating and a local Current Drive (CD) in a small radial range. Using this property, an ECW System is applicable for the stabilization of Neoclassical Tearing Modes (NTMs). NTMs are magnetic islands driven by the helical perturbation of (missing) bootstrap current on the rational flux surfaces. A seed magnetic island may be triggered by sawtooth crash or other mechanisms. If an island is large enough to flatten the pressure profile, the bootstrap current will be further reduced and thus, the mode becomes destabilized. On one hand, the threshold pressure ratio β for triggering the seed islands can be controlled [1]. On the other hand, the ECW system can

tune the local current and temperature profiles, as well as compensate the missing bootstrap current [2], to stabilize or suppress the mode.

To effectively stabilize and suppress the mode, the ECW deposition should be close to the flux surface where the island is located. Since an accurate real-time mapping of magnetic coordinates in view of sensors to the launcher parameters can be demanding, the optimum location for the deposition is usually found by trial-and-error. Therefore, the ECW system should be capable of fast tuning the deposition locations. The deposition takes place when the EC resonant condition

$$f_{\mathrm{res}} = N \frac{|B\, e|}{\gamma\, m_0} + k_{\parallel}\, v_{\parallel} \tag{1}$$

is fulfilled, where e is the electron charge and m_0 the rest mass of an electron, γ is the Lorentz factor, $N = 1, 2, 3 \ldots$ is the harmonic EC frequency number, $k_{\parallel}$ and $v_{\parallel}$ are the wave number and electron velocity along the magnetic field.

Typically, the injected well-focused ECW beams have a fixed frequency f_{beam}. Taking the poloidal injection angle α_{beam} and toroidal angle β_{beam} as variables, ideally, each combination of $(\alpha_{\mathrm{beam}}, \beta_{\mathrm{beam}})$ corresponds to a resonant location at $f_{\mathrm{beam}} = f_{\mathrm{res}}$ on the beam path. Varying α_{beam} and β_{beam} independently, a surface of resonances can be defined for the given frequency. In a well-designed system, this surface crosses multiple nested flux surfaces of the confined plasma within a small range of injection angles. Therefore, moving the ECW deposition to a different flux surface can be achieved by tilting the launcher mirrors, like in ASDEX-Upgrade [3], DIII-D [4], FTU [5], JT-60U [6], TCV [7], TEXTOR [8], Tore Supra [9], etc. They are categorized as "angular steering" in this context. These approaches include:

- Front steering (e.g. ITER upper launcher [10, 11]) involves fast tilting of water-cooled heavy mirrors close to the plasma. The mechanics must tolerate high neutron loading.

- Remote steering, as in the Wendelstein 7-X stellarator, lacks the flexibility in terms of beam focusing and system integration, as the Talbot effect [12] requires for a given frequency a certain length of straight antenna waveguide, where bending is only possible perpendicular to the plane of steering. The waveguide in W7-X is longer than 6 m [13]. If the section size would be the same, the antenna waveguide in DEMO should be even longer.

- Mid-steering is currently being investigated for the integration in DEMO. Compared to the front steering, the steering mechanics are recessed behind the breeding blanket. This is the fixed-frequency steering variant for DEMO [14].

Another method to tune the deposition location is the so called "frequency step-tuning" [15]. This is the tunable-frequency variant currently investigated for DEMO as alternative solution. It is based on the principle that the dominating toroidal magnetic field $|B_{\mathrm{t}}| \propto R^{-1}$. Therefore, different R coordinates along a fixed beam path correspond to different resonant frequencies according to eq. (1). In this approach, the ECW frequency is tuned instead of the injection angles. Dynamically movable mirrors close to the plasma can be avoided. The simplification of launcher integration by having no actuators would have so significant advantages that it is worth to generally check the basic feasibility and usability of such a frequency step-tunable ECW system for NTM stabilization. The NTM stabilization has the toughest localization requirements for Electron Cyclotron Current Drive (ECCD). If the step tuning works for NTM, it will very probably also work for the other requirements.

The basic design considerations and the principle feasibility of a frequency step-tunable system will be discussed. They are arranged in the following sections by components. The transmission system is excluded from the discussions since it is in principle sufficiently broadband and probably not the showstopper for the whole system. The Brewster-angle torus window with large diamond disk is a critical component, which faces challenges in common with the gyrotron output window and will be briefly addressed there.

In section 2, the considerations of frequency step-tunable fusion gyrotrons will be summarized. Characteristic parameters will be assumed based on the current technological developments. Section 3 shows the considerations on the tuning of deposition profiles in the reference plasma scenario [16]. To consider the assumptions and parameters altogether, simulation cases for the envisaged NTM stabilization strategy are presented in section 4.

2. Considerations on frequency step-tunable gyrotrons

Gyrotrons are the microwave sources of the ECW system. The essential geometries and parameters of a gyrotron are illustrated in fig. 1. A recent comprehensive review of fusion gyrotrons is given in [17], while the state-of-the-art can be found in [18]. The discussions in this section will focus on the frequency step-tuning.

The frequency of the generated microwaves is determined by eq. (1). Since the interaction between the electron beam and the microwave in a gyrotron takes place slightly above the cut-off frequencies of the cavity modes, the Doppler term $k_{\parallel} v_{\parallel}$ of a gyrotron is insignificant. Therefore, the fundamental microwave frequency is approximately the relativistic EC frequency

$$f \approx \frac{B_{\text{cavity}}}{\text{T}} \frac{28\ \text{GHz}}{\gamma} \tag{2}$$

The Lorentz factor can be expressed using the beam voltage U in kV:

$$\gamma = 1 + \frac{U}{511\,\text{kV}} \tag{3}$$

where U of gyrotron electron beams is typically 80–90 kV. Very high order cavity modes guarantee manageable ohmic losses. Usually, a gyrotron is optimized only for a single operating frequency. There are also frequency-tunable gyrotrons, e.g. [19–23], which are capable of outputting multiple frequencies at high power. A frequency tunable ECW system for NTM stabilization will need the gyrotron operating frequencies to be dense and roughly equidistant, in order to achieve a fast sweeping of ECW deposition in a quasi-continuous range of flux surfaces.

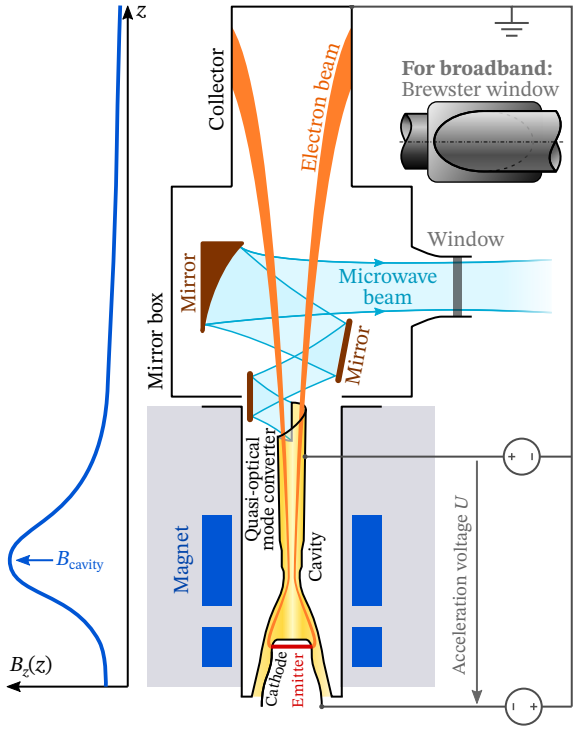

Fig. 1: Schematic of a gyrotron

Although the frequency could be changed by tuning the resonant structure mechanically [24], it is however more realizable to adjust the EC frequency by changing the magnetic field B and acceleration voltage U, as summarized in [25–27]. Only tuning U in eq. (3) is not practical, because it hardly affects γ for a gigahertz frequency variation, while the cavity modes have high resonant quality factors in discrete frequency steps of 2–3 GHz. Typically, the variation of frequency is accomplished mainly by tuning the cavity magnetic field. The gyrotron magnetic field is tuned via ramping the current in the (auxiliary) Normal-Conducting (NC) or Super-Conducting (SC) windings. The ramping speed of the magnet determines the frequency tuning speed.

A very fast tuning speed of 652 mT/s ($\hat{=}$ 15 GHz/s) was achieved by a hybrid gyrotron magnet [19]. There, an NC coil was used for sweeping. However, this hybrid magnet works only in 1 ms pulses with a duty cycle of 0.1 %. This is not suitable for the application of NTM stabilization for the reason explained in section 4. In 2008, the 7 T cryogen-free magnet [28] by JASTEC was able to apply 40 mT/s tuning speed in a range of $\pm$ 200 mT, corresponding to 0.96 GHz/s for a total bandwidth of approximately 9.6 GHz. The tuning speed and range of this JASTEC magnet will be considered here as typical characteristics.

The 2 MW coaxial gyrotron in [29] is taken here as reference for the possible cavity modes and frequencies. Its operation at 170 GHz in the $\text{TE}_{34,19}$ mode has been experimentally validated. Since DEMO might need above 200 GHz (e.g. estimated in [30]) for a highly efficient ECCD at the plasma center, the frequency tunability in the vicinity of 204 GHz was theoretically studied [31]. For NTM stabilization, the frequency around 170 GHz is currently specified [14, 32]. At the time of writing, the tunability for 170 GHz is under investigation. Therefore, assumptions will be made based on the characteristics

from [31]. The assumptions and simplifications for a 170 GHz tunable gyrotron are as follows:

- Since the choice of cavity modes for the tuning of the reference gyrotron was not finalized, totally 7 modes from $TE_{31,19}$ to $TE_{37,19}$ with the same radial index are assumed. It is possible that a few of them should be replaced by other modes with different radial indices. The operating frequencies are approximated by the cold cavity resonant frequencies which are $f =$ 163.68, 165.79, 167.90, 170.02, 172.13, 174.24, and 176.34 GHz. This total bandwidth corresponds to a gyrotron magnetic field range of roughly ±260 mT, which is larger but in the same order as the reference range.

- The optimization of the interaction power (here, the limitation is the ohmic loss) depends on the magnetic field. For simplification, the power is assumed to be independent of the magnetic field, as qualitatively visualized in fig. 2.

- A characteristic ramping speed of 40 mT/s is assumed according to [28]. Scanning the total bandwidth would take 13 s.

- The optimum operating magnetic field for each mode is assumed from eq. 2, where $\gamma \approx 1.16$. A gap of 40 mT is reserved between the neighboring modes. This number is qualitatively assumed based on the diagram in [31]. It is illustrated in fig. 2. When the magnetic field being ramped lies inside these gaps, the gyrotron should be turned off. The ramping time of the gyrotron magnet field over one gap interval is 1 s under the assumed conditions. This becomes approximately the time scale for adjusting the polarizers and matching optical units, as well as tuning the disk distance if variable-spacing double-disk windows would be used.

Other considerations on the frequency step-tunable gyrotrons include the output Gaussian fundamental mode content and the broadband window. The internal quasi-optical mode converter converts the TE cavity mode to a linearly polarized fundamental Gaussian mode, which is transmitted through the output window. The mode content may not be always optimum for all designed cavity modes. Typical simulated values of the mode content in tunable gyrotrons can be found in e.g. [33, 34]. It

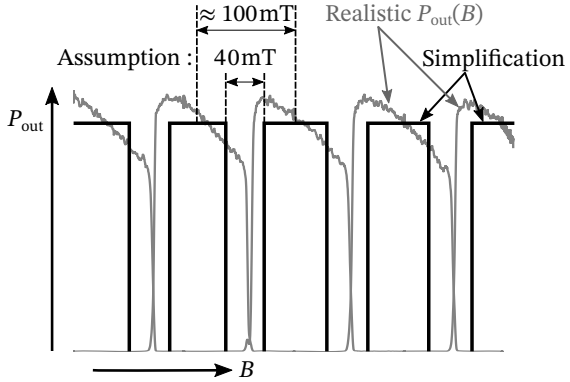

Fig. 2: Assumptions and simplifications of the gyrotron frequency tuning behavior for the simulation studies in section 4. The realistic curves are the ones published in [31]. Though it is based on the 204 GHz operation points, the general considerations are also applicable for 170 GHz.

is possible for some frequencies that the current mode converter would provide an output beam with a Gaussian mode content lower than 95 %, where this number was specified in ITER. A careful choice of mode series and optimization of the converter design are necessary for fulfillment of this mode purity requirement.

Brewster windows made from various materials, such as SiN, BN or Chemical Vapor Deposition (CVD) diamond, have been experimentally validated in megawatt-class step-tunable gyrotrons [35–37] up to 3 ms pulses. However, targeting Continuous Wave (CW) high power gyrotron operations, CVD diamond is the only possible choice as window material for the disk, thanks to its unique combination of extraordinary thermal, mechanical and optical properties. Unfortunately, differently from the standard window configuration (perpendicular to the beam direction), for the same window aperture, large area diamond disks are required in the Brewster-angle configuration (tilted by 67.2°). Currently, in close contact with industrial partners, several diamond growth experiments are ongoing with very promising results aiming at a 180 mm diameter, crack-free, optical grade diamond disk [38, 39] with approximately 2 mm thickness. This target represents the first challenge to solve in the Brewster window development. Then, looking at the window manufacturing, the next challenge refers to the asymmetric brazing between such disks and the copper boundary. From the perspective of the microwave, a challenge to face is the potential arcing in CW gyrotrons operation [17, 40]. In case of showstoppers for this development path, a fall-back solution would be the variable-spacing double-disk

window, like in the multi-frequency system of ASDEX Upgrade [41], but optimized for the DEMO frequency band and tuning speed.

3. Considerations on the discrete tunable ECW depositions for NTM control

The current baseline parameters of the European DEMO are summarized in [16]. The NTMs with $(m, n) = (3, 2)$ and $(2, 1)$ are critical, where m and n are poloidal and toroidal mode number, respectively. Based on the ECW system at the time of writing [14], there will be dedicated NTM launcher antennas. Moreover, two sets of launchers aim individually at the rational surfaces of the $(3, 2)$ and $(2, 1)$ modes. Therefore, the demanded steering range for NTMs in DEMO might not be so wide as in an experimental machine like ITER.

In this part of the present study, TORBEAM [42, 43] is used to calculate the achievable CD profiles, steering range and steering resolution of a frequency tunable setup in the nominal plasma scenario [16]. The current NTM launcher parameters [14] are taken as reference in the following way. To simplify the setup, a single ECW beam will represent the aggregated beams targeting one NTM flux surface. The same launcher positions as in the current mid-steering configuration are adopted. However, the launching angles need to be modified, in order to achieve a nearly uniform radial coverage with the discrete deposition profiles. The beams are focused using mirrors, which are compatible to the current mid-steering design.

The poloidal projections of the frequency-tunable beams are shown in fig. 3. The red dots mark the locations of the EC resonances at the center frequency (170.02 GHz) including the Doppler up-shift. When the ECW frequency is tuned in steps, the resonance jumps discretely along the beam path within a local interval. In order to deposit the ECW onto different flux surfaces, the beam should cross multiple surfaces within the interval of resonances. For this reason, the beams cannot be too tangential to the flux surfaces. Therefore, the deposition width is broader and the CD may be less efficient than the optimized angular steering setups, which can be seen in fig. 4.

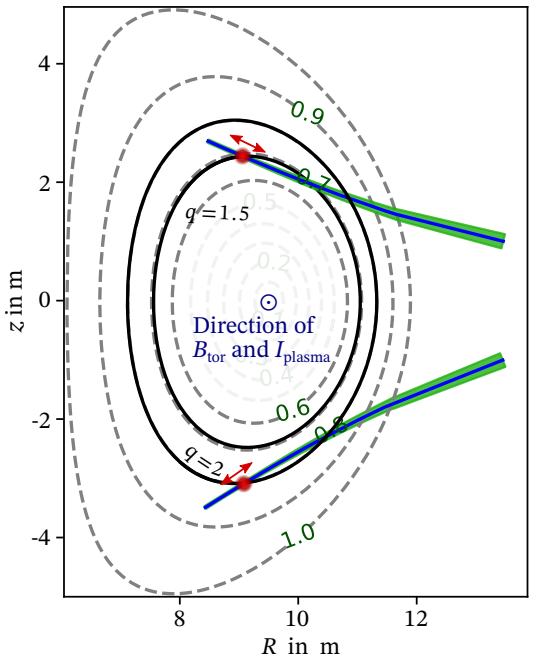

Fig. 3: The ECW beams for stabilization of NTMs. The upper beam is aimed at the $(3, 2)$ mode, the lower at the $(2, 1)$ mode. Both fractional surfaces are marked with solid black curves. The flux labels are ρ_{pol}.

The curves with rainbow-order colors in fig. 4 are the CD density profiles of one ECW beam, where the colors correspond to the gyrotron frequencies. All CD densities are normalized to 1 MW injected power. To demonstrate that the neighboring beams can also be aimed at the same locations in the given scenario, the CD profiles of a neighboring beam are shown as dotted curves. Taking the more critical $(2, 1)$ NTM for example, the average distance between the peaks of two neighboring deposition profiles is 0.0083 in ρ_{pol}, while the profile full width at $1/e$ of amplitude is 0.011. The deposition width projected on the equatorial axis (≈ 3 cm) in this case is more localized than the width (6 cm) specified by the current DEMO guideline, in absence of beam broadening. At a different launching position and with another injection angle, the steering range can be doubled, at the expense of doubling the profile widths from 3 to 6 cm (thus, lower peak CD) and doubling the distance between the profile peaks. To keep the compatibility with the other works, the following simulation studies will still be based on fig. 4 at this stage.

There are two main uncertainties in this assumed configuration. First, the scenario presented here is only for a general check, as DEMO is still under an early phase of development. Second, the beam might be up to a factor

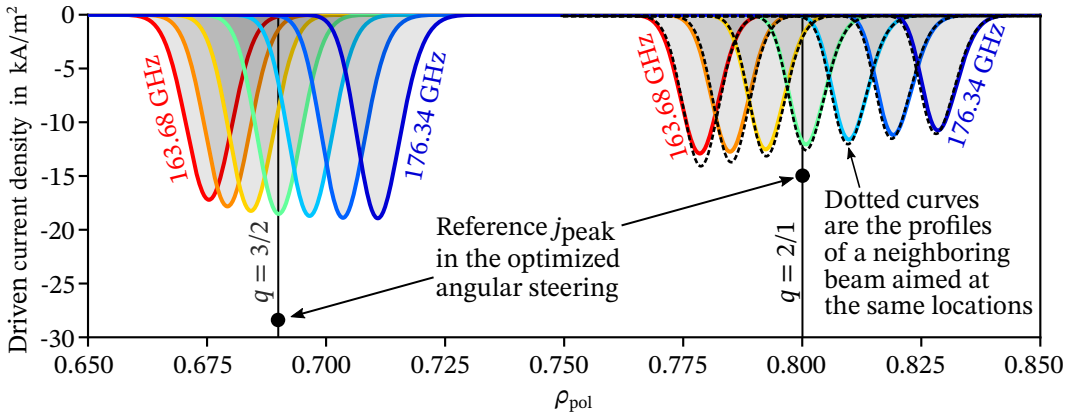

Fig. 4: Current drive density profiles calculated by TORBEAM. Negative sign of CD in the diagram means co-ECCD. The injected ECW power is normalized to 1 MW for each frequency step. Colors of curves correspond to frequencies in the mode series given in section 2.

of 4 broader due to the fluctuation of electron density [44]. The beam broadening is still to be verified in medium size experimental tokamaks and properly extrapolated in view to ITER and DEMO.

4. Simulation study of NTM control model with step-tunable ECW system

To demonstrate the properties of the frequency tunable ECW system, the control of the $(m, n) = (2, 1)$ NTM is simulated based on the nominal DEMO plasma scenario [16] using ASTRA [45]. An ideal ECW beam targeting the $q = 2$ surface is taken for example, as explained in section 3. Since the ECW power is assumed constant during one simulation, the inputs of the NTM stabilization system are the magnetic field of gyrotrons and the ECW power on/off switch. The schematic of the simulation is shown in fig. 5, which re-uses a part of the code base from [46]. A seed island is triggered artificially by adding a truncated Gaussian profile to the electron perpendicular heat diffusivity $\chi_\perp$. The width of the truncated profile represents the seed island size. A high $\chi_\perp$ will remove the local gradient of the pressure. With the assumed plasma parameters, the mode is destabilized in the absence of ECCD for $w_{seed} \gtrsim 3\,\mathrm{cm}$. In each iteration of the loop, the island evolution is updated and the MHD equilibrium is solved simultaneously in axisymmetric approximation.

The NTM growth and stabilization have been modeled in numerous works e.g. [3, 47–53]. In this study, the mode growing speed $(\mathrm{d}\,w/\mathrm{d}\,t)$ is formulated as

$$\mathcal{I}_1 \frac{\mu_0\, r_s}{\eta} \frac{\mathrm{d}\,w}{\mathrm{d}\,t} = r_s \left(\Delta' + \Delta'_{BS} + \Delta'_{CD} + \Delta'_{H}\right) \qquad (4)$$

where the dimensionless factor $\mathcal{I}_1$ is the integral from eq. (112) of [49], η is the electrical resistivity and r_s is the radius of the rational surface, which is approximated in this study by $r_s \approx a\,\rho_{tor}$, where a is the equatorial minor radius. The formulation of the bootstrap term is adapted from [49, 51, 52, 54], but the polarization part is not included at this stage:

$$\Delta'_{BS} \propto f_{GGJ}\,\beta_p \sqrt{\frac{r_s}{R_0}} \frac{L_q}{L_p} \frac{w}{w^2 + w_d^2} \qquad (5)$$

where $f_{GGJ} \lesssim 1$ is given in eq. (12.4) of [54], β_p is the pressure normalized to poloidal magnetic field pressure at

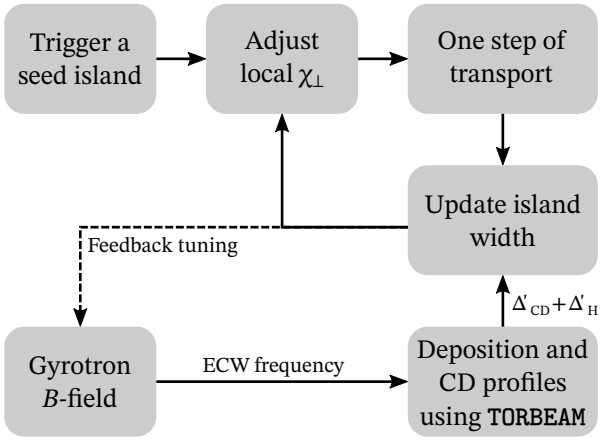

Fig. 5: Schematic of the NTM control simulation in ASTRA

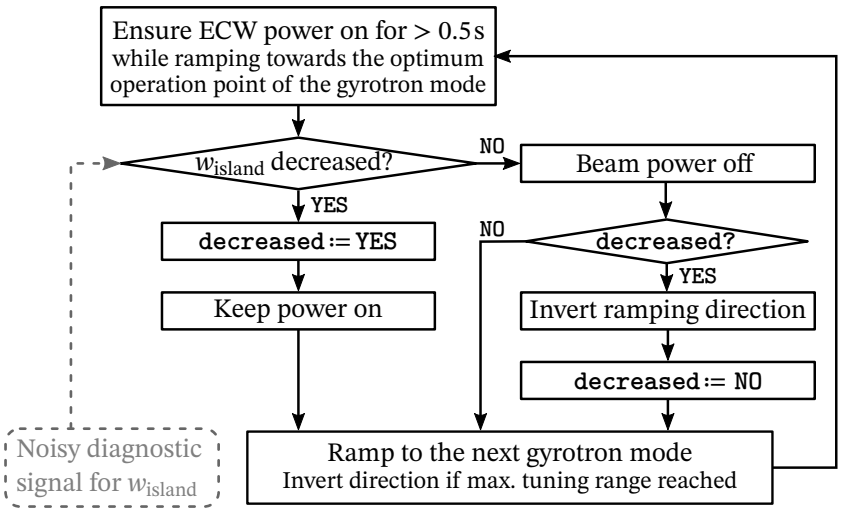

Fig. 6: A simple sweeping strategy for the NTM control. The ramping of gyrotron magnetic field starts from one boundary of the sweeping range and does not stop even when the deposition is already aligned with the island. The sweeping direction is reversed when the step is not effective, or the sweeping boundary is reached.

the rational surface, $L_q = q/(\mathrm{d}\,q/\mathrm{d}\,r)$ and L_p is defined in the same way. The last fraction of eq. (5) has a maximum when the island width $w = w_\mathrm{d}$, where w_d is derived in [49]. Substituting with the assumed plasma parameters results in $w_\mathrm{d} \approx 4$–$5\,\mathrm{cm}$. Since there is no experimental data to calibrate the model; following the calculations in [53], a guess for the saturated island size is 40–50 cm. This assumption is used to determine the proportionality coefficient of eq.(5).

The Δ'_CD term of eq. (4) is given in [50, 52]:

$$\Delta'_\mathrm{CD} = -\frac{16\,\mu_0}{\pi\, s\, B_\mathrm{pol}}\,\frac{I_\mathrm{CD}}{w_\mathrm{depo}^2}\,F_\mathrm{CD} \tag{6}$$

where $s = r_\mathrm{s}/L_q$ is the shear; I_CD and w_depo are evaluated from the profiles calculated by TORBEAM. The fit term F_CD for a CW ECCD is based on the formulation in [52]. The Δ'_H term is also taken from [52]:

$$\Delta'_\mathrm{H} = -\frac{16\,\mu_0}{\pi\, s\, B_\mathrm{pol}}\,\frac{I_\mathrm{H}}{w_\mathrm{depo}^2}\,F_\mathrm{H} \tag{7}$$

considering the fit term F_H for CW from [55], where the current I_H is caused by the perturbation of electron temperature profile. The effect of Δ'_H is negligible compared to Δ'_CD in the given plasma scenario.

Taking the CD efficiency from fig. 4 for an ECW power of 19 MW (the power is a provisional assumption), the maximum possible width of a perfectly aligned ECCD profile, which can still suppress the (2,1) NTM in this model is approximately 0.05 in ρ_tor, i.e. 15 cm on the equatorial axis. In general, the requirement of deposition width should be much smaller than the width estimated from the perfect alignment and the requirement also depends on the control strategy.

The strategy of NTM control considered in this study does not assume an accurate equilibrium reconstruction nor an in-line-ECE [8], such that the optimum ECW frequency cannot be directly obtained from diagnostics. Instead, the optimum is found by "search and suppress" like in [56]. An adapted "search and suppress" method for frequency step-tuning is shown in fig. 6. Basically, it is a sweeping of the frequency. The decision of sweeping direction is based on whether the island size has decreased. The reason for such a strategy is that, due to the conservative assumptions of uncertainties in diagnostics and NTM models, an adequate dwell time of ECW deposition with sufficient power is necessary to ensure a correct searching decision. Therefore, the pulsed frequency tuning [19] mentioned in section 2 is not suitable. The typical dwell time is in the order of 100 ms [56] to 1 s. For DEMO, a minimum dwell time of 0.5 s is preliminarily assumed based on the current physics understanding and expected DEMO diagnostics features. A better guess might be extrapolated from ITER experiments. In the present simulations, the dwell time is variable (due to the different distances between gyrotron modes) but at least 0.5 s is ensured. Besides, the magnitude of the stabilization terms in eq. (4) is also crucial for the decision. In other words, if the power is not enough to drive a sufficient

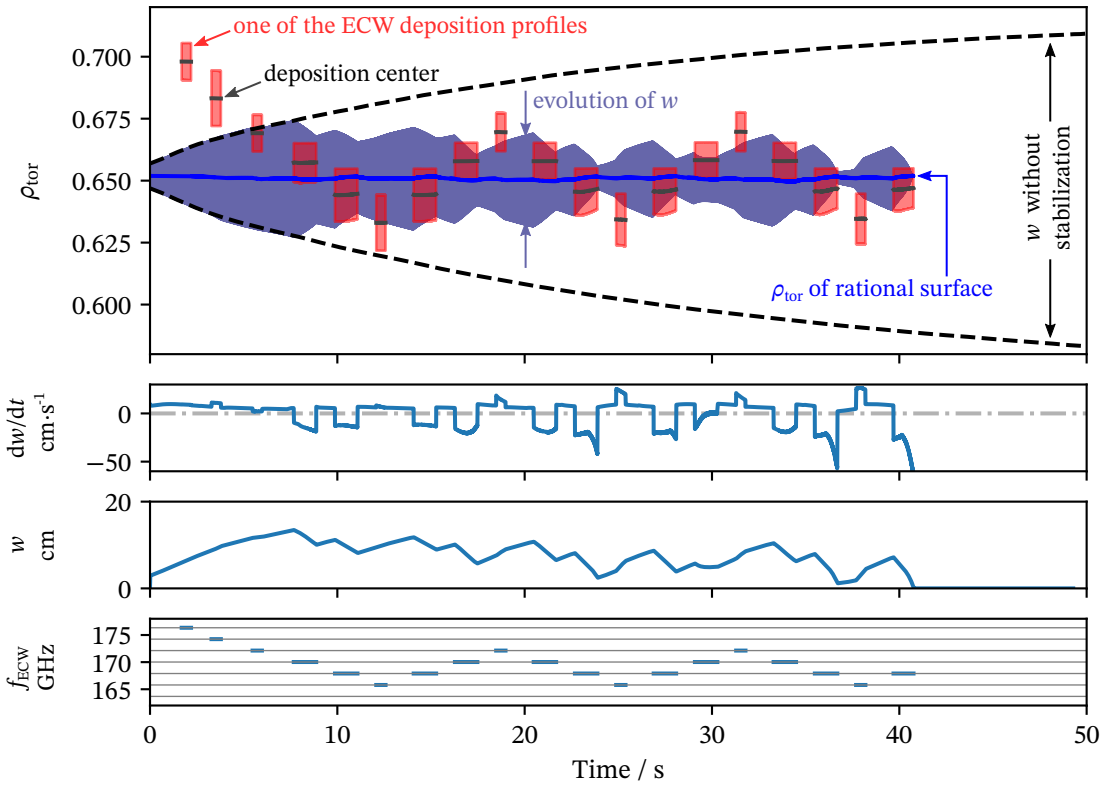

Fig. 7: Simulation of NTM stabilization using 19 MW ECW power. Compared to fig. 4, the flux label $\rho_{\mathrm{tor}} = 0.65$ corresponds to $\rho_{\mathrm{pol}} = 0.8$. The launching angle is deviated from fig. 4, in order to avoid a perfect alignment.

current, the island does not shrink; in this case, a correct searching decision cannot be made either. Therefore, it is considered in the strategy that the entire ECW power for an NTM should be applied on one profile. On the other hand, if the total power could be split into multiple depositions simultaneously by controlling each beam frequency individually, it might be useful for advanced control strategy, but this is not applied here due to the uncertainties. Another compromise in this control strategy is that the sweeping of frequency is continuing, although the island already shrinks. This could be improved by using an adaptive sweeping amplitude, as shown in [46].

The evolutions of the $(2, 1)$ NTM and ECW depositions are shown in fig. 7. In order to consider an imperfect alignment between deposition profiles and the rational surface, a small deviation is added to the launching angle on purpose, so that the $q = 2$ surface is not at the center of any profile. The sweeping of the frequency starts from one boundary of the frequency band when $w_{\mathrm{island}} > 6\,\mathrm{cm}$. The island width $w \ll 3\,\mathrm{cm}$ at 41 s such that the NTM is considered as completely suppressed. It can be seen in the figure that the sweeping strategy shown in fig. 6 should be further improved, especially for the following reasons

- Once the sweeping passes through the island, the driven current is just outside of the island separatrix and the mode grows faster.
- Within the assumed 40 mT gap in fig. 2, the ECW power is off and the mode starts again to grow. The gap makes the overall suppression less effective.
- The continuous ramping of gyrotron magnetic field in the assumed speed would require back-and-forth pumping of stored magnetic energy in a speed of 10–20 kW. This power is roughly estimated from the variation of stored energy in the (not fast-tunable) magnet of [29] as if there was only the main SC coil. No resistive loss or inducted current in other coils is considered.

Based on the assumptions, there will be no concrete improvement of control strategy at this stage. For the assumed NTM model and launcher configuration, with on-and-off switching an injected ECW power of 19 MW

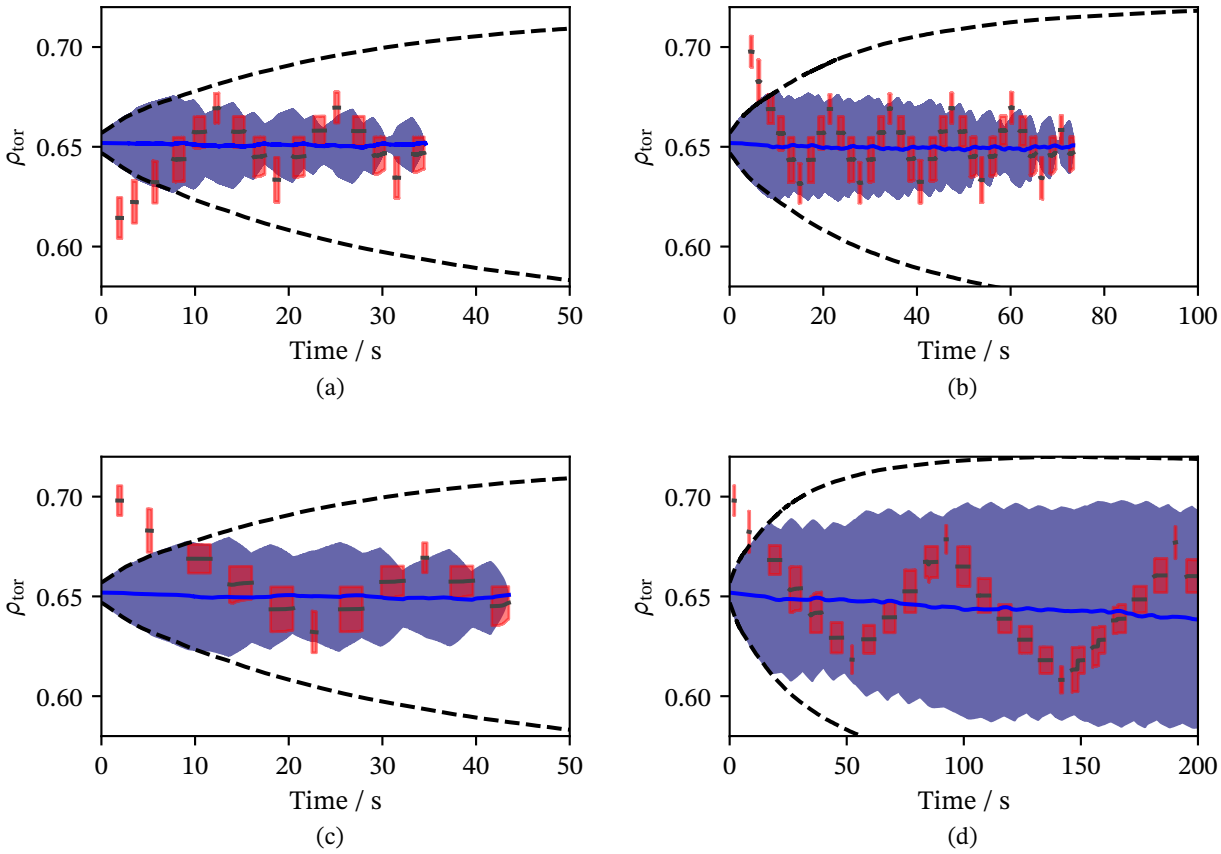

Fig. 8: Additional simulation cases with 19 MW ECW power. (a) The sweeping starts from a lower frequency. (b) The sweeping is switched on when the initial $w_{\mathrm{island}} = 10\,\mathrm{cm}$. (c) The ramping speed is reduced to 20 mT/s. (d) The ramping speed is reduced to 10 mT/s (fails to stabilize the mode).

and a minimum dwell time of 0.5 s, it is sufficient to overcome the maximum island growth when $w \approx w_{\mathrm{d}}$. At the operation point of fig. 7, increasing the ECW power in steps of 2 MW will reduce the time requirement for the suppression by 8 s in average.

Four additional simulation cases are presented in fig. 8. Figure 8(a) shows the case when the sweeping starts from the lower boundary. Here, the ramping speed is the same as in fig. 7. Another case, where the sweeping starts when $w_{\mathrm{island}} = 10\,\mathrm{cm}$ instead of 6 cm, is shown in fig. 8(b). The suppression in this case takes longer time. However, the stabilization will fail if the start of sweeping is further delayed. The case for a halved ramping speed of gyrotron magnet is shown in fig. 8(c). If the ramping speed is slowed down to one fourth of the reference speed, the mode based on the present model cannot be suppressed using the simple sweeping strategy. This is shown in fig. 8(d).

Since the model is based on the currently available assumptions and approximations, the requirement of ECW power, ramping speed and the time needed for the suppression are only qualitative expectations. Besides, the beam broadening and mode locking will introduce further uncertainties. These effects impact also the angular steering methods and they are not specific for frequency step tuning. The margin in the present scenario is not enough for beam broadening by factor higher than 2 if the ECW power is not increased. Mode locking should be considered in the next phase of modeling.

5. Conclusion

A frequency step-tunable ECW system can avoid mechanics for dynamically tilting the ECW launcher mirrors close to plasma. However, the estimation of its feasibility needs to match the technical possibilities and the physics requirement.

This study considers a reasonable generalization and extrapolation of the current frequency step-tunable gyrotron technology. The realizable ramping speed of the gyrotron magnetic field is a limiting factor of the system. In order to operate in multiple frequencies, the gyrotron optimizations have to tolerate the trade-offs for the output power per tube and the fundamental Gaussian mode content, which further decreases the effective ECW power.

The optimization of ECW launching angles and launcher positions depends on the plasma scenario. A technical design for the EC launcher is under study for the mid-steering antenna solution and therefore not needed to be studied further here except for a simplification to remove the actuators and to exchange movable to fixed mirrors. From the current reference launching positions, a steering range of $\rho \gtrsim 0.05$ could be achievable with 7 frequency steps. A broader steering range may also be possible with the same number of steps, by optimizing the launching positions. However, there are trade-offs between the steering resolution, steering range, CD intensity and susceptibility to the deviation of plasma scenarios.

NTM stabilization using frequency step-tunable ECW are modeled and simulated. The simulation takes into account the previous assumptions of gyrotrons and launching parameters. A simple sweeping strategy of ECW frequency is applied. Simulations of the model show that, the opportunity to suppress NTMs in DEMO using a step-tunable ECW system with the currently achievable technologies exists. However, the uncertainties in the assumptions need to be further investigated. Also, more robust feedback control modeling is needed and the optimization of the control algorithm is a future goal.

Acknowledgement

This work has been carried out within the framework of the EUROfusion consortium and has received funding from the Euratom research and training programme 2014–2018 and 2019–2020 under grant agreement No 633053. The views and opinions expressed herein do not necessarily reflect those of the European commission.

A. Snicker was supported by the Academy of Finland (Grant No. 324759).

References

[1] O. Sauter et al., Control of neoclassical tearing modes by sawtooth control, Physical Review Letters 88 (10) (2 2002). doi:10.1103/physrevlett.88.105001.

[2] G. Gantenbein et al., Complete suppression of neoclassical tearing modes with current drive at the electron-cyclotron-resonance frequency in ASDEX upgrade tokamak, Physical Review Letters 85 (6) (2000) 1242–1245. doi:10.1103/physrevlett.85.1242.

[3] H. Zohm et al., Neoclassical tearing modes and their stabilization by electron cyclotron current drive in ASDEX Upgrade, Physics of Plasmas 8 (5) (2001) 2009–2016. doi:10.1063/1.1344564.

[4] E. Kolemen et al., State-of-the-art neoclassical tearing mode control in DIII-D using real-time steerable electron cyclotron current drive launchers, Nuclear Fusion 54 (7) (2014) 073020. doi:10.1088/0029-5515/54/7/073020.

[5] A. Bruschi et al., ECRH antenna at 140 GHz on FTU tokamak, Fusion Engineering and Design 53 (1-4) (2001) 431–441. doi:10.1016/s0920-3796(00)00517-2.

[6] A. Isayama et al., Complete stabilization of a tearing mode in steady state high-β_p H-mode discharges by the first harmonic electron cyclotron heating/current drive on JT-60U, Plasma Physics and Controlled Fusion 42 (12) (2000) L37–L45. doi:10.1088/0741-3335/42/12/102.

[7] S. Alberti et al., Third-harmonic, top-launch, ECRH experiments on TCV tokamak, Nuclear Fusion 45 (11) (2005) 1224–1231. doi:10.1088/0029-5515/45/11/002.

[8] B. A. Hennen et al., Real-time control of tearing modes using a line-of-sight electron cyclotron emission diagnostic, Plasma Physics and Controlled Fusion 52 (10) (2010) 104006. doi:10.1088/0741-3335/52/10/104006.

[9] M. Lennholm et al., The ECRH/ECCD system on Tore Supra, a major step towards continuous operation, Nuclear Fusion 43 (11) (2003) 1458–1476. doi:10.1088/0029-5515/43/11/019.

[10] R. Chavan et al., The ECH front steering launcher for the ITER upper port, Fusion Engineering and Design 82 (5-14) (2007) 867–872. doi:10.1016/j.fusengdes.2007.05.035.

[11] D. Strauss et al., Nearing final design of the ITER EC H&CD upper launcher, Fusion Engineering and Design 146 (2019) 23–26. doi:10.1016/j.fusengdes.2018.11.013.

[12] H. F. Talbot, I. facts relating to optical science. No. III, The London, Edinburgh, and Dublin Philosophical Magazine and Journal of Science 9 (51) (1836) 1–4. doi:10.1080/14786443608636441.

[13] B. Plaum et al., High-power tests of a remote steering launcher mock-up at 140 GHz, Journal of Physics: Conference Series 25 (2005) 120–129. doi:10.1088/1742-6596/25/1/016.

[14] T. Franke et al., Integration concept of an electron cyclotron system in DEMO, Fusion Engineering and Design 168 (2021) 112653. doi:10.1016/j.fusengdes.2021.112653.

[15] H. Zohm et al., On the use of step-tuneable gyrotrons in ITER, Journal of Physics: Conference Series 25 (2005) 274–282. doi:10.1088/1742-6596/25/1/033.

[16] M. Siccinio et al., DEMO physics challenges beyond ITER, Fusion Engineering and Design 156 (2020) 111603. doi:10.1016/j.fusengdes.2020.111603.

[17] M. K. A. Thumm et al., High-power gyrotrons for electron cyclotron heating and current drive, Nuclear Fusion 59 (7) (2019) 073001. doi:10.1088/1741-4326/ab2005.

[18] M. Thumm, State-of-the-art of high-power gyro-devices and free electron masers, Journal of Infrared, Millimeter, and Terahertz Waves 41 (1) (2020) 1–140. doi:10.1007/s10762-019-00631-y.

[19] K. Koppenburg et al., Fast frequency-step-tunable high-power gyrotron with hybrid-magnet-system, IEEE Transactions on Electron Devices 48 (2001) 101–107. doi:10.1109/16.892175.

[20] V. E. Zapevalov et al., Development of a prototype of a 1-MW 105-156-GHz multifrequency gyrotron, Radiophysics and Quantum Electronics 47 (5/6) (2004) 396–404. doi:10.1023/b:raqe.0000046313.84364.3c.

[21] R. Ikeda et al., Development of multi-frequency gyrotron for ITER and DEMO at QST, in: 41st International Conference on Infrared, Millimeter, and Terahertz waves, IEEE, 2016. doi:10.1109/irmmw-thz.2016.7758384.

[22] D. S. Tax et al., Experimental results for a pulsed 110/124.5-GHz megawatt gyrotron, IEEE Transactions on Plasma Science 42 (5) (2014) 1128–1134. doi:10.1109/tps.2014.2314019.

[23] A. Samartsev et al., Efficient frequency step-tunable Megawatt-class D-band gyrotron, IEEE Transactions on Electron Devices 62 (7) (2015) 2327–2332. doi:10.1109/ted.2015.2433016.

[24] G. F. Brand et al., Continuously tunable, split-cavity gyrotrons, International Journal of Infrared and Millimeter Waves 6 (1985) 1237–1254. doi:10.1007/bf01013212.

[25] O. Dumbrajs et al., Fast frequency-step-tunable gyrotrons for plasma heating and fusion diagnostics 26 (1994) 561–565. doi:10.13182/fst94-a40216.

[26] O. Dumbrajs, Tunable gyrotrons for plasma heating and diagnostics, Riga Aviation Universit Scientific Reports Computer Modeling & New Technologies 2 (1998) 66–70.

[27] M. Thumm et al., Frequency step-tunable (114–170 GHz) megawatt gyrotrons for plasma physics applications, Fusion Engineering and Designs 53 (2001) 407–421. doi:10.1016/s0920-3796(00)00519-6.

[28] R. Hirose et al., Development of 7 T cryogen-free superconducting magnet for gyrotron, IEEE Transactions on Applied Superconductivity 18 (2008) 920–923. doi:10.1109/tasc.2008.922296.

[29] T. Rzesnicki et al., 2.2-MW record power of the 170-GHz European preprototype coaxial-cavity gyrotron for ITER, IEEE Transactions on Plasma Science 38 (6) (2010) 1141–1149. doi:10.1109/tps.2010.2040842.

[30] E. Poli et al., Electron-cyclotron-current-drive efficiency in DEMO plasmas, Nuclear Fusion 53 (1) (2012) 013011. doi:10.1088/0029-5515/53/1/013011.

[31] T. Ruess et al., Theoretical study on the possibility for stepwise tuning of the frequency of the KIT 2 MW 170/204 GHz coaxial-cavity gyrotron, in: 45th International Conference on Infrared, Millimeter, and Terahertz Waves, IEEE, 2020. doi:10.1109/irmmw-thz46771.2020.9370801.

[32] G. Granucci et al., Conceptual design of the EU DEMO EC-system: main developments and R&D achievements, Nuclear Fusion 57 (11) (2017) 116009. doi:10.1088/1741-4326/aa7b15.

[33] O. Prinz et al., Quasi-optical mode converter for a multi-frequency D-band gyrotron, in: Joint 32nd International Conference on Infrared and Millimeter Waves and the 15th International Conference on Terahertz Electronics, IEEE, 2007. doi:10.1109/icimw.2007.4516778.

[34] P. C. Kalaria et al., RF behavior and launcher design for a fast frequency step-tunable 236 GHz gyrotron for DEMO, Frequenz 71 (3-4) (Jan. 2017). doi:10.1515/freq-2016-0212.

[35] O. Braz et al., D-band frequency step-tuning of a 1 MW gyrotron using a Brewster output window, International Journal of Infrared and Millimeter Waves 18 (8) (1997) 1465–1477. doi:10.1007/bf02678305.

[36] G. G. Denisov et al., Multi-frequency gyrotron with BN Brewster window, in: Joint 31st International Conference on Infrared Millimeter Waves and 14th International Conference on Teraherz Electronics, IEEE, 2006. doi:10.1109/icimw.2006.368283.

[37] G. Gantenbein et al., First operation of a step-frequency tunable 1-MW gyrotron with a diamond Brewster angle output window, IEEE Transactions on Electron Devices 61 (6) (2014) 1806–1811. doi:10.1109/ted.2013.2294739.

[38] G. Aiello et al., Diamond window technology for electron cyclotron heating and current drive: state of the art, Fusion Science and Technology 75 (7) (2019) 719–729. doi:10.1080/15361055.2019.1643690.

[39] G. Aiello et al., Large area diamond disk growth experiments and thermomechanical investigations for the broadband brewster window in DEMO, IEEE Transactions on Electron Devices 68 (9) (2021) 4669–4674. doi:10.1109/ted.2021.3088077.

[40] G. S. Nusinovich et al., The gyrotron at 50: historical overview, Journal of Infrared, Millimeter, and Terahertz Waves 35 (4) (2014) 325–381. doi:10.1007/s10762-014-0050-7.

[41] D. Wagner et al., Status of the new multi-frequency ECRH system for ASDEX upgrade, Nuclear Fusion 48 (5) (2008) 054006. doi:10.1088/0029-5515/48/5/054006.

[42] E. Poli et al., TORBEAM, a beam tracing code for electron-cyclotron waves in tokamak plasmas, Computer Physics Communications 136 (1-2) (2001) 90–104. doi:10.1016/s0010-4655(01)00146-1.

[43] E. Poli et al., TORBEAM 2.0, a paraxial beam tracing code for electron-cyclotron beams in fusion plasmas for extended physics applications, Computer Physics Communications 225 (2018) 36–46. doi:10.1016/j.cpc.2017.12.018.

[44] A. Snicker et al., The effect of density fluctuations on electron cyclotron beam broadening and implications for ITER, Nuclear Fusion 58 (1) (2017) 016002. doi:10.1088/1741-4326/aa8d07.

[45] G. V. Pereverzev et al., ASTRA automated system for transport analysis in a tokamak, Tech. Rep. IPP 5/98, Max-Planck-Institut für Plasmaphysik, Garching (2002). https://doi.org/11858/00-001M-0000-0027-4510-D

[46] R. Schramm, Development of a control system for neoclassical tearing modes in the European DEMO fusion reactor, Master's thesis, LMU (2020).

[47] P. H. Rutherford, Nonlinear growth of the tearing mode, Physics of Fluids 16 (11) (1973) 1903. doi:10.1063/1.1694232.

[48] Z. Chang et al., Observation of nonlinear neoclassical pressure-gradient-driven tearing modes in TFTR, Physical Review Letters 74 (23) (1995) 4663–4666. doi:10.1103/physrevlett.74.4663.

[49] R. Fitzpatrick, Helical temperature perturbations associated with tearing modes in tokamak plasmas, Physics of Plasmas 2 (3) (1995) 825–838. doi:10.1063/1.871434.

[50] O. Sauter, On the contribution of local current density to neoclassical tearing mode stabilization,

Physics of Plasmas 11 (10) (2004) 4808–4813. doi:10.1063/1.1787791.

[51] R. J. La Haye, Neoclassical tearing modes and their control, Physics of Plasmas 13 (5) (2006) 055501. doi:10.1063/1.2180747.

[52] D. D. Lazzari et al., On the merits of heating and current drive for tearing mode stabilization, Nuclear Fusion 49 (7) (2009) 075002. doi:10.1088/0029-5515/49/7/075002.

[53] O. Sauter et al., On the requirements to control neoclassical tearing modes in burning plasmas, Plasma Physics and Controlled Fusion 52 (2) (2010) 025002. doi:10.1088/0741-3335/52/2/025002.

[54] H. Zohm, Magnetohydrodynamic stability of tokamaks, Wiley-VCH GmbH, 2014.

[55] D. D. Lazzari et al., On the merits of heating and current drive for tearing mode stabilization, Nuclear Fusion 50 (7) (2010) 079801. doi:10.1088/0029-5515/50/7/079801.

[56] C. Rapson et al., Amplitude based feedback control for NTM stabilisation at ASDEX upgrade, Fusion Engineering and Design 89 (5) (2014) 568–571. doi:10.1016/j.fusengdes.2014.01.007.